NAIM and Site-Specific Functional Group Modification Analysis of RNase P RNA: Magnesium Dependent Structure within the Conserved P1−P4 Multihelix Junction Contributes to Catalysis†

Nicholas M. Kaye, Eric L. Christian, and Michael E. Harris*

Center for RNA Molecular Biology, Case Western Reserve University School of Medicine, Cleveland, Ohio 44106

Received December 14, 2001; Revised Manuscript Received January 24, 2002

ABSTRACT: The tRNA processing endonuclease ribonuclease P contains an essential and highly conserved RNA molecule (RNase P RNA) that is the catalytic subunit of the enzyme. To identify and characterize functional groups involved in RNase P RNA catalysis, we applied self-cleaving ribozyme−substrate conjugates, on the basis of the RNase P RNA from *Escherichia coli*, in nucleotide analogue interference mapping (NAIM) and site-specific modification experiments. At high monovalent ion concentrations (3 M) that facilitate protein-independent substrate binding, we find that the ribozyme is largely insensitive to analogue substitution and that concentrations of Mg^{2+} (1.25 mM) well below that necessary for optimal catalytic rate (>100 mM) are required to produce interference effects because of modification of nucleotide bases. An examination of the pH dependence of the reaction rate at 1.25 mM Mg^{2+} indicates that the increased sensitivity to analogue interference is not due to a change in the rate-limiting step. The nucleotide positions detected by NAIM under these conditions are located exclusively in the catalytic domain, consistent with the proposed global structure of the ribozyme, and predominantly occur within the highly conserved P1−P4 multihelix junction. Several sensitive positions in J3/4 and J2/4 are proximal to a previously identified site of divalent metal ion binding in the P1−P4 element. Kinetic analysis of ribozymes with site-specific N7-deazaadenosine and deazaguanosine modifications in J3/4 was, in general, consistent with the interference results and also permitted the analysis of sites not accessible by NAIM. These results show that, in this region only, modification of the N7 positions of A62, A65, and A66 resulted in measurable effects on reaction rate and modification at each position displayed distinct sensitivities to Mg^{2+} concentration. These results reveal a restricted subset of individual functional groups within the catalytic domain that are particularly important for substrate cleavage and demonstrate a close association between catalytic function and metal ion-dependent structure in the highly conserved P1−P4 multihelix junction.

Ribonuclease P (RNase P)[1] catalyzes the hydrolysis of a specific phosphodiester bond in tRNA precursors to generate the mature tRNA 5′ end. A distinguishing feature of this class of tRNA processing endonucleases is an essential and highly conserved RNA subunit (RNase P RNA) (*1*, *2*) that is the catalytic subunit of the enzyme (*3*). Like other large ribozymes (Group I and Group II self-splicing introns), RNase P RNA catalyzes phosphoryl transfer and has an absolute requirement for divalent metal ions (*1*, *2*). Although several structural motifs, such as loop−helix interactions, can be found in all three large ribozyme classes, the conserved sequence and structural features that define them are distinct. To understand how RNase P RNA achieves catalysis and the properties it shares with other RNA and protein enzymes, it is essential to identify individual functional groups that contribute to catalysis and to determine their specific roles.

High-resolution structural information concerning the RNase P enzyme−substrate complex is not yet available; however, a reasonably detailed perspective on elements of RNase P RNA structure involved in substrate binding and catalysis is provided by biochemical studies. The RNase P ribozyme is thought to be composed of two domains (*4*, *5*): a substrate binding or S-domain that interacts with the T-stem and loop of tRNA (*6*−*11*) and a catalytic or C-domain that interacts with the base of the acceptor stem (*12*−*17*) and presumably contains the binding site for catalytic metal ions (Figure 1A). Structure probing studies identified several elements of the C-domain that contact the acceptor stem or are adjacent to the cleavage site and, so, appear to constitute a portion of the enzyme active site. Conserved nucleotides within the C-domain at J5/15 and J18/2 cross-link to photoagents positioned at or near the G(+1)−C(+72) basepair in the pre-tRNA substrate (*12*−*14*). In addition, the

† This work was supported by NIH Grant GM56740 to M.E.H.

* Corresponding author. Phone: (216) 368-4779. Fax: (216) 368-3055. E-mail: meh2@pop.cwru.edu.

[1] Abbreviations: RNase P, ribonuclease P; NAIM, nucleotide analogue interference mapping; EDTA, ethylenediamine tetraacetate; PIPES, piperazine-*N*,*N*′-bis(2-ethanesulfonic acid); C-domain, catalytic domain; S-domain, substrate binding domain; AαS, adenosine-α-phosphorothioate; GαS, guanosine-α-phosphorothioate; PurαS, purine-α-phosphorothioate; 2APαS, 2-aminopurine-α-phosphorothioate; DAPαS, 2,6-diaminopurine-α-phosphorothioate; ^{NME}AαS, N6-methyladenosine-α-phosphorothioate; 7dAαS, N7-deazaadenosine-α-phosphorothioate; IαS, inosine-α-phosphorothioate; dA, 2′-deoxyadenosine; N7dA, N7-deaza-2′-deoxyadenosine; N7dG, N7-deaza-2′-deoxyguanosine.

10.1021/bi012158h CCC: $22.00
Published on Web 03/15/2002

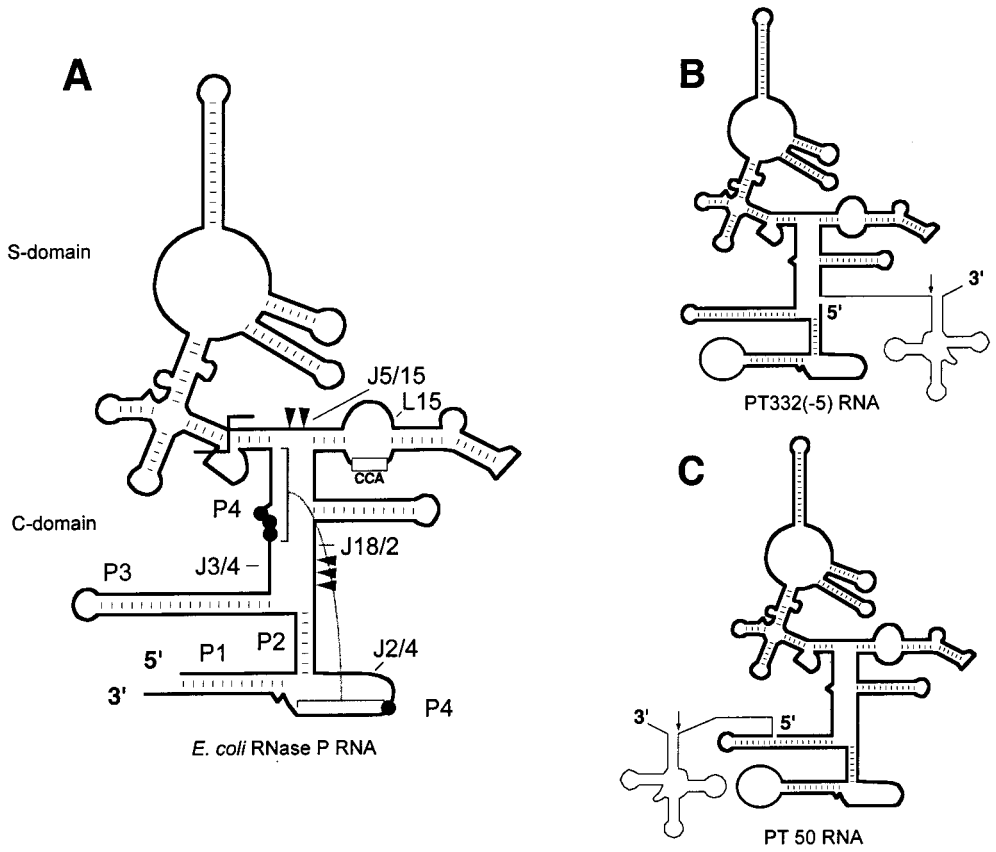

FIGURE 1: Secondary structures of native *E. coli* RNase P RNA, PT332(-5), and PT50. (A) Diagram of the native *E. coli* RNase P RNA secondary structure. Helices are designated as P (paired) and numbered from the 5′ end. Regions between helices are designated as J (joining), and numbered based on the helical elements that they connect. The helices and joining regions referred to in the text are indicated. Helix P4 is shown as brackets connected by a line. Nucleotides where phosphorothioate modification interferes with substrate binding (*37*) and catalysis are shown as black circles. Positions of nucleotides detected by 5′ photoagent-modified tRNA (*12*−*14*) are indicated by gray arrows. The nucleotides in P15 that interact with the 3′-CCA sequence of tRNA (*15*−*17*) are indicated by a box. Secondary structures of the PT332(-5) ribozyme (B) and the PT50 ribozyme (C) are shown (*22*, *30*). RNase P RNA sequences are shown as a dark line, and tRNA and linker sequences are shown as thinner lines. The self-cleavage site generating mature tRNA is designated by an arrow.

conserved 3′-CCA sequence of tRNA interacts with a loop or internal bulge adjacent to P15 (*15*−*17*). The small RNase P protein, which is essential for enzyme function in vivo, has been demonstrated to bind to conserved RNase P RNA elements within the C-domain (*18*) and is involved in recognizing the pre-tRNA 5′ leader sequence (*19*, *20*). However, despite the extensive evidence for close association between the pre-tRNA cleavage site and elements of the C-domain, a complete understanding of the ribozyme active site architecture, in particular the role of essential metal ion interactions, is still lacking.

There is growing evidence that the conserved helix P4 in the C-domain is one of the binding sites for magnesium (Mg^{2+}) ions that is important for catalysis. Phosphorothioate modifications at nucleotides A67, G68, and A352 in *Escherichia coli* RNase P RNA result in greater than 1000-fold decreases in the rate of catalysis (*21*, *22*) (Figure 1A). The effect of sulfur substitution on rate for modifications at A67 can be rescued by soft metal ions such as manganese and cadmium, providing evidence for direct coordination of metal ions within P4 (*22*). Additionally, specific point mutations within P4 increase ribozyme activity in the presence of calcium, further supporting a role in metal ion interactions (*23*) (Kaye et al., submitted for publication). P4 is part of a larger structural element within the C-domain, encompassing helices P1−P4, a multihelix junction that is unique to RNase P RNA and conserved in enzymes from all three phylogenetic domains (*24*, *25*). Collectively, the proximity of the P1−P4 junction to the pre-tRNA cleavage site and the evidence for functional metal ion binding in P4 suggests that this motif may play a direct role in enzyme catalysis. However, it has been difficult to deconvolute the structure of this multihelix junction from the available biochemical data, and the binding sites for functionally important metal ions in P1−P4 are not well understood.

To investigate the structural and biochemical basis for RNase P ribozyme function, we undertook a series of nucleotide analogue interference mapping (NAIM) experiments to identify functional groups involved in catalysis. NAIM utilizes α-thiophosphate-tagged nucleotide analogues to identify, by modification−interference, individual chemical groups involved in nucleic acid function (*26*). This approach has proven to be a particularly powerful method for determining the chemical basis of RNA structure and function including RNA−RNA interactions, monovalent ion interactions, and nucleotide base ionization (for example, see refs *27*−*29*). Application of this approach allowed for the identification of purine N7, guanosine N2, ribose-2′-hydroxyl, and nonbridging phosphate oxygens in the RNase P ribozyme that are important for substrate binding and catalysis (*21*, *30*−*35*). These studies collectively demonstrate that functional groups involved in substrate binding are found

in both the catalytic and substrate-binding domains, in general occurring in regions which can form intermolecular cross-links with photoagent-modified pre-tRNA substrates. Interference experiments utilizing gel-mobility shift approaches to examine functional groups important for substrate binding provided important insights into elements of tertiary structure as well (*34*). However, significantly less information is available concerning the specific functional groups that participate directly in substrate cleavage. Of particular interest are residues and functional groups that contribute to essential metal ion interactions in the C-domain because they are likely to play a central role in substrate recognition and catalysis.

To better understand these issues, NAIM and site-specific functional group modification experiments were employed to identify functional groups that contribute to RNase P ribozyme catalysis. These studies detected a small subset of functional groups at universally conserved nucleotide positions in J3/4, J5/15, J18/2, and J2/4 within the C-domain. Interestingly, low concentrations of divalent metal ions, relative to the optimal concentrations for the ribozyme reaction, were required to detect analogue interference, suggesting coupling of the interference effects to relatively high-affinity metal ion binding. Importantly, analysis of the pH dependence of the self-cleavage reactions indicated that the increased sensitivity to analogue substitution at low Mg^{2+} concentration was not due to a change in a rate-limiting step. Several of the functional groups identified here cluster in J3/4 and J2/4 near phosphorothioate-sensitive backbone positions in P4 that are involved in divalent metal ion coordination. Site-specific modifications of purine N7 functional groups in J3/4 confirm the NAIM results and permit a more detailed investigation of the effect of these modifications on metal ion dependence. We find that deleterious effects of N7 modification at A62, A65, and A66 in J3/4 can be suppressed at higher Mg^{2+} concentrations but display very distinct sensitivities to metal ion concentration. These studies provide insight into the participation of specific functional groups in substrate cleavage and suggest that the metal ion-dependent structure in the highly conserved P1−P4 multihelix junction is important for ribozyme catalysis.

MATERIALS AND METHODS

RNA Synthesis and Construction of Site-Specifically Modified Ribozymes. Plasmid pPT332(-5) used to generate unmodified PT332(-5) RNA was generously supplied by the laboratory of Dr. Norman Pace. Plasmids pPT50, pG73PT50, and pG364PT332 used to generate PT50, G73PT50, and G364PT332 RNAs are described elsewhere (*22*).

Uniformly labeled RNA was synthesized by in vitro transcription of linearized plasmids by T7 RNA polymerase (80 units) in 40 mM Tris-HCl (pH 7.9), 6 mM $MgCl_2$, 2 mM spermidine, 10 mM DTT (polymerase and buffer from Ambion), and 1 mM rATP, rCTP, rUTP, and rGTP at 37 °C for 6 h. To generate RNAs suitable for 5′ end labeling or ligation (e.g., G73PT50 and G364PT332(-5)), transcription conditions were as those described previously except guanosine was added to 6 mM. Transcribed RNAs were subsequently ethanol-precipitated, resuspended in an equal volume of 1 mM EDTA and a gel loading buffer (98% formamide, 10 mM EDTA (pH 8.0), 0.025% xylene cyanol FF, and 0.025% bromophenol blue), heated to 90 °C for 2 min, and purified on a 6% (19:1) polyacrylamide (8 M urea) gel. Labeled RNAs were visualized by autoradiography, while unlabeled RNAs were visualized by UV shadowing. RNAs were excised from the gel and eluted in a 5−10-fold volume excess of elution buffer (40 mM Tris-HCl (pH 7.5), 1 mM EDTA, 0.3 M sodium acetate, and 0.1% sodium dodecyl sulfate) for 4−12 h. Eluted RNAs were extracted twice with an equal volume of a 1:1 mixture of phenol and chloroform, extracted once with an equal volume of chloroform, and then precipitated with three volumes of ethanol.

The oligonucleotides and reaction conditions used to generate site-specifically modified PT50 ribozymes by oligonucleotide-directed ligation are described in Christian et al. (*22*). Briefly, RNA fragments encompassing nucleotides 50−73 that contained the appropriate modification were joined to the remaining RNase P RNA sequences that were generated by in vitro transcription. The 5′-oligoribonucleotide was radiolabeled with γ32P-ATP and polynucleotide kinase, and the appropriate ligation fragment was purified by polyacrylamide gel electrophoresis, as described previously. Unmodified RNAs and RNAs containing 2′-deoxy modifications were from Dharmacon. Oligonucleotides with N7-deazaadenosine or N7-deazaguanosine were generated using modified deoxynucleotide phosphoramidites from Glenn Research at the nucleic acid synthesis facility at the University of Alabama, School of Medicine.

PT50 and PT332(-5) Ribozyme Reactions. Although experimental conditions were varied with respect to $MgCl_2$ concentration and pH, standard reactions were performed as follows. The general optimization of the self-cleavage reaction conditions has been described elsewhere (*36*). Six microliters of transcribed or ligated RNA (2 nM) in a solution containing 1 mM EDTA (and 0.1% NP-40 for ligated RNAs) was mixed with 48 μL of a stock reaction buffer (3.75 M NaCl and 62.5 mM PIPES (pH 5.5) at 50 °C) and annealed in a PTC-100 programmable thermal controller (MJ Research; 85 °C for 1 min, cooled to 65 °C at 0.2 °C/s, maintained at 65 °C for 5 min, cooled to 50 °C at 0.25 °C/s, and incubated for 3.5 h at 50 °C). Reactions were initiated by adding 6 μL of an appropriate 10*x* stock solution of $MgCl_2$. The final reaction conditions, excluding Mg^{2+}, were 0.2−2 nM RNA, 3 M NaCl, and 50 mM PIPES (pH 5.5) at 50 °C. $MgCl_2$ was mixed into the solution by rapid pipetting; 6 μL aliquots were removed at various times and quenched by mixing with gel loading buffer containing a 2:1 excess of EDTA relative to $MgCl_2$ (typically, 10 mM EDTA, 98% formamide). Products were loaded directly onto 6% polyacrylamide (8 M urea) gels and visualized by phosphorimager analysis (Molecular Dynamics).

Analysis of Reaction Kinetics. The pseudo-first-order reaction rate constant (k_{obs}) was determined by fitting plots of the fraction of RNA cleaved as a function of time to an equation for a single-exponential

$$\frac{[P]}{[S]_{total}} = A - Be^{-k_{obs}t} \quad (1)$$

where $[P]/[S]_{total}$ is the ratio of the radioactivity in the product band to the total radioactivity in both the precursor and product RNAs, *A* represents the maximal extent of the reaction, and *B* is the amplitude of the exponential. However, approximately 5−20% of the precursor RNAs does not

cleave at incubation times up to 60 min. The majority of this initially unreactive fraction is resolved into the appropriate reaction products in 5−14 h. For such long time courses, the data were better fit by an equation for a double-exponential increase as follows:

$$\frac{[P]}{[S]_{total}} = A - (Be^{-k_1 t} + Ce^{-k_2 t}) \quad (2)$$

where k_1 represents the larger rate constant, k_2 represents the smaller rate constant, A represents the maximal extent of the reaction, and B and C are the amplitudes of the two exponentials. Plots of k_{obs} versus $[Mg^{2+}]$ were fit with a nonlinear form of the Hill equation for cooperative binding

$$k_{obs} = \frac{k_{max}[Mg^{2+}]^n}{(K_{Mg}^{app})^n + [Mg^{2+}]^n} \quad (3)$$

where k_{obs} is the pseudo-first-order rate constant determined at different Mg^{2+} concentrations using eq 1 and n is the Hill coefficient, which gauges the cooperativity of Mg^{2+} binding ($n = 1$ represents no cooperativity). K_{Mg}^{app} is the Mg^{2+} concentration required to attain half of the maximal rate (k_{max}).

Nucleotide Analogue Interference Mapping. Phosphorothioate nucleotide analogues of purine (PurαS), 2-aminopurine (2APαS), 2,6-diaminopurine (DAPαS), N6-methyladenosine (^{NME}AαS), N7-deazaadenosine (7dAαS), and inosine (IαS) were incorporated into PT332(-5) RNA at a level of approximately one modification per molecule, as described previously (*37*). Modified ribozymes were subsequently cleaved under the conditions described in the text. Reacted and unreacted RNAs were separated on 6% polyacrylamide gels. RNAs were recovered by elution from the gel and ethanol precipitation as described previously and resuspended at ca. 50 000 CPM/μL in 10 mM Tris-HCl (pH 8.0) and 0.5 mM EDTA. I_2 was used to cleave end-labeled RNAs at sites of phosphorothioate modification (*38*, *39*). Approximately 100 000 CPM of labeled RNA in 2 μL was combined with 2 μL of a 1:500 dilution (in water) of 0.1 M iodine (in ethanol) for a final concentration of 0.05 mM I_2. After an incubation at 95 °C for 2 min, 4 μL of a solution containing 80% formamide, 0.05% bromophenol blue, and 0.05% xylene cyanol FF was added, and the 95 °C incubation continued for an additional 2 min. A 1−2 μL aliquot of the sample was loaded on a 6% or 10% denaturing acrylamide gel containing 8 M urea and was analyzed as described previously.

Intensities of bands corresponding to adenosine or guanosine phosphorothioate (NαS) modification and for nucleotide analogue (δαS) modification for each position in the reacted and unreacted populations were quantified using a Molecular Dynamics phosphorimager and ImageQuant software. The extent of interference (I) for each position, normalized for phosphorothioate effects and variability in analogue incorporation, was calculated using these values in the following equation (*26*):

$$I = \frac{(\delta\alpha S_{reacted}/\delta\alpha S_{unreacted})}{(A\alpha S_{reacted}/A\alpha S_{unreacted})} \quad (4)$$

The normalized interference values (κ) were obtained by dividing each individual interference value by the average interference value for each position within two standard deviations of the mean. This operation normalizes all interference data, where $\kappa = 1$ indicates no interference, values greater than one indicate interference, and values lower than one indicate an enhancement of activity because of analogue incorporation. The normalized interference values for the nucleotide identified in the text were 2 or greater.

RESULTS

NAIM Analysis of Functional Groups Important for RNase P Ribozyme Catalysis. The self-cleaving RNase P ribozymes (PT332(-5) and PT50) employed in these studies contain circularly permuted RNase P ribozyme sequences covalently joined via a short oligonucleotide linker to tRNA sequences (Figure 1, parts B and C). The attachment points are based on intermolecular cross-linking results which position the 5′ leader of pre-tRNA near J18/2 and the proximal portion of P3 (*13*, *14*). Both ribozymes were previously shown to react via intramolecular cleavage at the correct phosphodiester bond (*22*, *30*, *36*). Figure 2 shows representative kinetic data for the PT332(-5) and PT50 self-cleavage reactions. Intramolecular cleavage of 5′-^{32}P-labeled RNA results in the formation of an unlabeled 3′ fragment that is the mature tRNA and a 5′ fragment containing the ribozyme sequences, which can be easily isolated from the precursor population by gel electrophoresis (Figure 2, parts A and B). Plots of the fraction of RNA reacted versus time fit well to single-exponential functions, yielding rate constants ($k_{obs} = 0.73$ and 0.74 min^{-1} for PT332(-5) and PT50, respectively) (Figure 2C) that are essentially identical to that of the single turnover reaction of the native *E. coli* ribozyme at 37 °C under similar pH and mono- and divalent ion conditions ($k_{obs} = 0.87$ min^{-1}) (*22*).

The ability to separate active from inactive molecules on the basis of their self-cleavage activity permits the application of chemical interference approaches. To identify ribozyme functional groups that contribute to substrate cleavage, we employed a series of adenosine and guanosine phosphorothioate analogues in NAIM experiments (Figure 3A). These reagents were previously used to analyze ribozyme functional groups involved in substrate binding (*34*, *35*, *37*, *40*) (Figure 3A). Thus, the analysis permits a comparison of the contribution of specific functional groups to these two aspects of enzyme function. Briefly, NAIM involves application of nucleotide analogues that contain alterations of one or a few chemical groups that are covalently tagged with a 5′-phosphorothioate (*26*). Analogues are incorporated into RNA by in vitro transcription, and the substituted populations are separated into active and inactive fractions on the basis of their ability to perform a particular function. In the present analysis, the RNAs were separated on the basis of their ability to catalyze intramolecular cleavage. Positions of analogue incorporation are determined by chemical cleavage at the phosphorothioate linkage (see Materials and Methods). Interference by analogue incorporation at a specific residue results in under-representation of modification at that position in the active population (Figure 3B). Because the α-phosphorothioate tag is necessary for locating the position of analogue incorporation, the few positions where the phos-

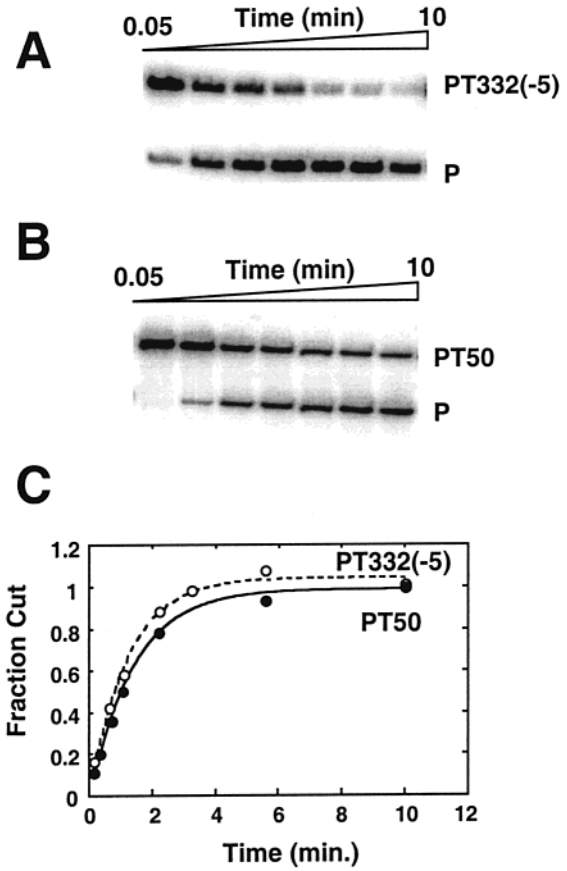

FIGURE 2: Kinetics of PT332(-5) and PT50 self-cleavage reactions. A and B show resolution by polyacrylamide gel electrophoresis of the products from reactions containing either 5′-^{32}P-end-labeled PT332(-5) or PT50, respectively. Reactions contained 2 nM 5′ end-labeled RNA, 25 mM $MgCl_2$, 3 M NaCl, 50 mM PIPES, (pH 5.5) and were carried out at 50 °C. The positions or bands corresponding to precursor (PT) or product (P) RNAs are indicated to the right of the gel. (C) Plot of the fraction ribozyme reacted versus time for PT332(-5) (open circles) and PT50 (filled circles) from Christian et al. (*22*). Data are fit to single-exponential functions (eq 1), yielding rate constants of 0.73 and 0.74 min^{-1} for PT332(-5) and PT50, respectively. The fits for PT50 and PT332(-5) are shown by solid and dashed lines, respectively.

phorothioate modification interferes with function can provide no further information concerning base modification.

The analogues applied here identify interference effects because of modification in the minor groove faces of adenine and guanine as well as the major groove face of adenine base (Figure 3A). Three analogues probe the N6 position: ^{NMe}AαS, 2APαS, and PurαS. While ^{NMe}AαS has one of the N6 amine hydrogens replaced by a methyl group, PurαS and 2APαS both lack the adenosine N6 amine. DAPαS and 2APαS have an additional amine group at the 2 position of the purine ring and, so, examine the tolerance of an additional functional group on the minor groove edge of the base. 7dAαS has a carbon atom in place of N7 and, thus, eliminates a potential hydrogen-bond acceptor or metal ion coordination site in the major groove. All of these analogues are accurately and efficiently incorporated into the *E. coli* RNase P RNA by in vitro transcription with T7 RNA polymerase (*30*, *37*).

In contrast to the strong interference signal due to modification of specific nonbridging phosphate oxygens reported previously (*21*) (at A67, G68, U69, and A352), we

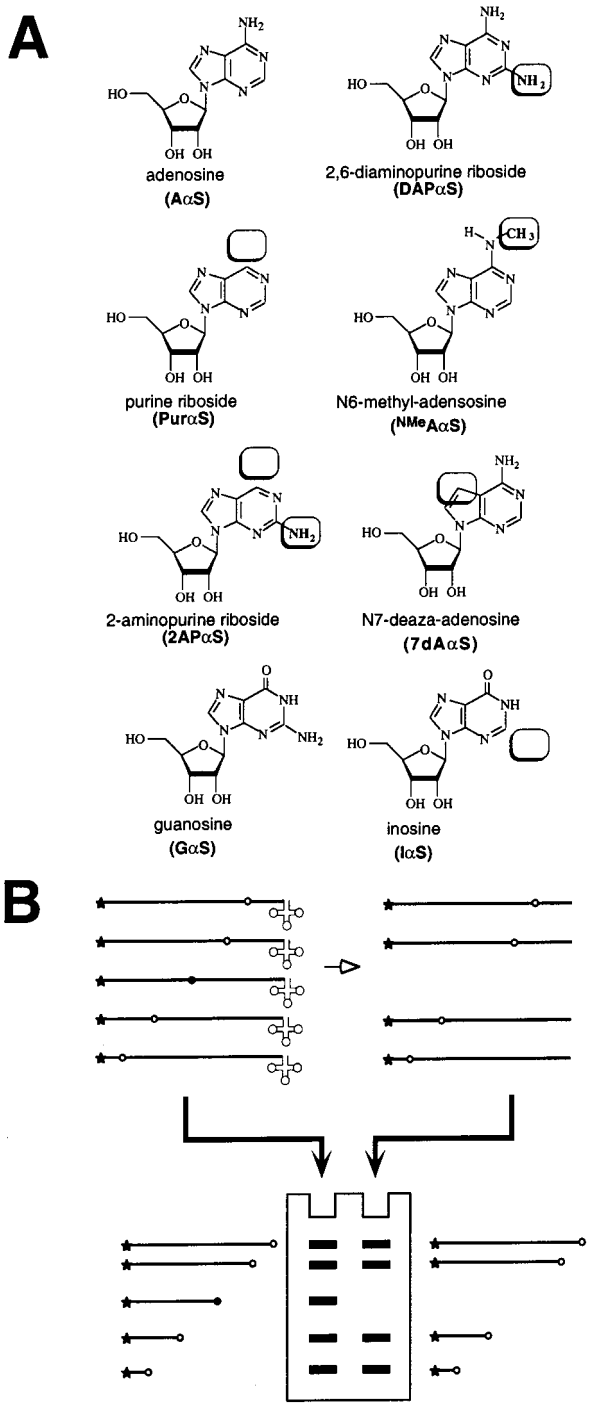

FIGURE 3: Nucleotide analogue interference mapping (NAIM) reagents and selection approach. (A) Chemical structures of the nucleotide analogues employed in these studies. Analogues are shown as nucleosides but are incorporated into RNA as the α-phosphorothioate derivative (*26*, *75*). Base functional groups that are modified relative to adenosine or guanosine are boxed. Abbreviations used in the text and in other figures are shown in parentheses. (B) Diagram of an overview of NAIM as applied using PT332(-5) or PT50. Tethered ribozyme substrate conjugates indicated by a thick straight line with associated cloverleaf tRNA undergo intramolecular cleavage to remove the 3′-terminal tRNA. RNAs are radioactively end-labeled, as indicated by stars and modified internally at on average one modification per RNA, as indicated by circles. Modifications that reduce the rate of self-cleavage, indicated by a filled circle, result in under representation of the modified RNA in the product population. Precursor and product RNAs are isolated and cleaved with iodine at positions of analogue incorporation and visualized by electrophoresis on a standard polyacrylamide sequencing gel.

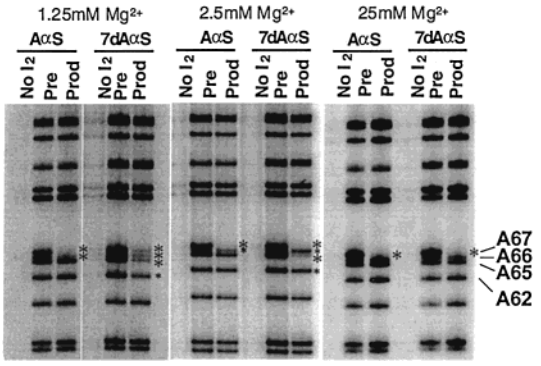

FIGURE 4: Mapping of AαS and 7dAαS interference effects in J3/4 and P4 at 1.25, 2.5, and 25 mM Mg^{2+}. Iodine cleavage products of 5′-^{32}P-end-labeled precursor and product RNAs were resolved by polyacrylamide gel electrophoresis. The metal ion concentrations employed in the cleavage selection and the analogues incorporated into the RNA are indicated above the gel. Lanes contain samples of precursor RNA that was mock treated with iodine (No I_2), or iodine cleavage products from precursor (Pre) or product (Prod) RNAs as indicated. Asterisks indicate individual nucleotide positions where interference effects were detected. The individual residue numbers are indicated to the right of the gel.

found no interference signal generated from modifications of the nucleotide base under the standard reaction conditions of 25 mM Mg^{2+} (Figure 4 and data not shown). However, using lower concentrations of Mg^{2+} employed in previous NAIM studies (1.25−2.5 mM) (*30*), significant interference effects ($\kappa > 2$, see Materials and Methods) attributable to modification of the nucleotide base were detected. An example of the increased sensitivity to base analogue interference at low Mg^{2+} concentration is shown in Figure 4 for 7dAαS interference at adenosines A62 and A65−A67 in helix P4. Figure 4 shows a comparison of the iodine cleavage patterns of the precursor and product populations obtained after a fixed fraction of the RNAs had reacted (50%) under conditions of 1.25, 2.5, and 25 mM Mg^{2+}. At 25 mM Mg^{2+}, a clear interference effect is observed for phosphorothioate modification at A67 because both AαS and 7dAαS give rise to interference effects. However, no additional interferences due to the incorporation of 7dAαS alone were detected under these conditions. In contrast, at 2.5 mM Mg^{2+}, A62 and A65−A67 all show sensitivity to 7dAαS incorporation. The interferences at A66 and A67 are due to phosphorothioate modification because they are observed with AαS-modified RNAs, while effects at A62 and A65 are due to modification of the N7 as these effects are only seen with the RNA modified with 7dAαS. Lowering the Mg^{2+} concentration to 1.25 mM does not result in any additional effects in this region, but the interferences at A62, and A65−A67 are more clearly observed.

As shown in Figure 6, we find that only a small subset of RNase P ribozyme nucleotides is sensitive to analogue substitution. Given the fraction of RNA allowed to react during selection (50%), we estimate that the single chemical substitutions at functionally important nucleotide base positions surveyed had only modest (ca. 2-fold) or no effect on the ribozyme reaction rate. In a first-order reaction, less than 50% cleavage of the precursor in 2 min corresponds to a rate lower than 0.35 min^{-1}, which would be at least 2-fold slower than the unmodified ribozyme rate (0.55 min^{-1}, pH 5.5, 25 mM Mg^{2+}; Table 1). Thus, under these conditions, we should, in principle, discern relatively small (2-fold)

Table 1: Effectes of Functional Group Modifications on Ribozyme Reaction Rate at 2.5 and 25 mM Mg^{2+}

	2.5 mM Mg^{2+}		25 mM Mg^{2+}	
ribozyme	$k_{obs}(min^{-1})$[a]	$k_{obs}^{mut}/k_{obs}^{wt}$	$k_{obs}(min^{-1})$	$k_{obs}^{mut}/k_{obs}^{wt}$
PT50	0.011 ± 0.001	1.0	0.55 ± 0.04	1.0
dA62[b]	0.013 ± 0.002	1.2	0.71 ± 0.04	1.3
N7dA62	0.0028 ± 0.0002	0.25	0.21 ± 0.01	0.38
N7dG63	0.014 ± 0.001	1.3	n/d	
dA65	0.010 ± 0.003	1.0	0.62 ± 0.02	1.1
N7dA65	0.0036 ± 0.0009	0.33	0.52 ± 0.05	0.95
dA66	0.063 ± 0.006	5.7	2.7 ± 0.2	4.9
N7dA66	0.037 ± 0.003	3.4 (0.59)[c]	1.7 ± 0.1	3.1 (0.63)
dA67	0.0083 ± 0.002	0.75	0.59 ± 0.03	1.1
N7dA67	0.016 ± 0.002	1.7	0.93 ± 0.05	1.7
N7dG68	0.026 ± 0.002	2.4	n/d	

[a] Rates were determined by fitting plots of fraction RNA reacted versus time to a single-exponential equation as described in Materials and Methods. The values reported represent the average and standard deviation from at least three independent trials. [b] The designation dA indicates a 2′-deoxyadenosine modification and N7dA and N7dG indicate N7-deaza-2′-deoxyadenosine and N7-deaza-2′-deoxyguanosine modifications, respectively. [c] The value shown in parenthesis is the effect of N7-deaza-2′-deoxyadenosine modification normalized to the stimulatory effect of 2′-deoxyadenosine modification at A66.

effects of analogue substitution on the self-cleavage reaction rate. This level of sensitivity is further supported by the analysis of the effects of site-specific functional group modifications (see the following discussion; Table 1).

As shown in Figures 5 and 6, we detect interferences at A62, A65, A249, A334, and A351 attributable to incorporation of the 7dAαS analogue. In addition, we detect interferences at A65 due to incorporation of 2APαS and PurαS, indicating that the deletion of the N6 group at this position affects function. However, ^{NMe}AαS does not interfere at this position, indicating that the function of the N6 at A65 tolerates the presence of a methyl group. Moreover, we find that incorporation of ^{NMe}AαS at A62, A249, A334, A347, and A361 gives rise to interference, indicating that N6-methylation at these positions is detrimental to function (Figure 5 and data not shown). Interestingly, of the five sites of 7dAαS interference, four of these positions (A62, A249, A334, and A351) are also sensitive to ^{NMe}AαS incorporation, suggesting a potential coordinate interaction with the major groove or Hoogsteen pairing face of these nucleotides. The DAPαS analogue resulted in interference at A334, A347, and A361 demonstrating that the minor groove edge of these bases is intolerant of introduction of an N2 amine. Additionally, interference by IαS was detected at G63 and G64, indicating that the N2 amines of these residues are important for ribozyme function (data not shown). Clearly, the functional groups detected by NAIM are important for ribozyme-mediated substrate cleavage. However, in contrast to the phosphorothioate effects in P4, nucleotide base modification only results in a significant decrease in reaction rate at very low (1.25 mM) Mg^{2+} concentrations.

Figure 6 shows a summary of the NAIM data obtained at 1.25 mM Mg^{2+}. We find that analogue-interference effects occur exclusively in the C-domain of the ribozyme at nucleotide positions that are conserved in bacterial RNase P RNAs. Additionally, there is significant overlap between these results and interference results identifying functional groups involved in substrate binding. Positions A62, G63, G64, A65−G68, A334, and A351 all show essentially

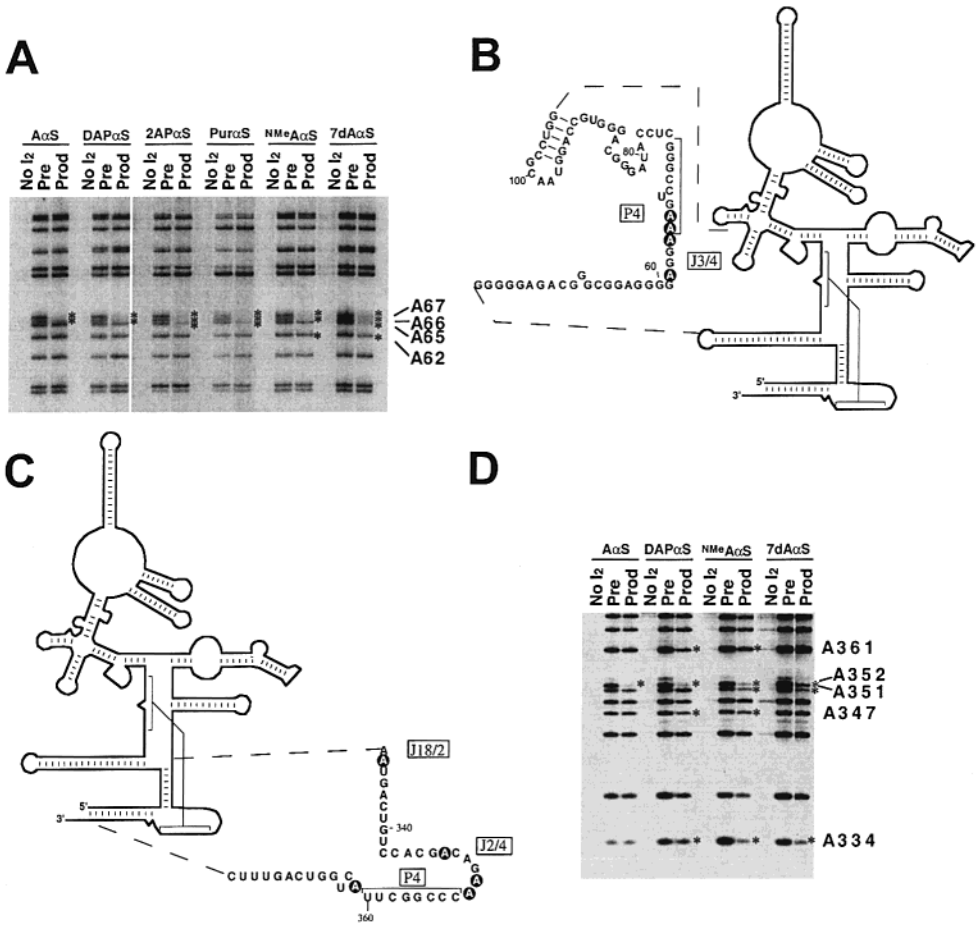

FIGURE 5: Mapping of analogue sensitive positions in the C-domain at low (1.25 mM) Mg^{2+} concentrations. (Panels A and D) Separation of iodine cleavage products of 5′-^{32}P-end-labeled RNA by polyacrylamide gel electrophoresis. The lane designations are the same as those used in Figure 4. Asterisks indicate the positions where significant interference effects were measured. The individual residue numbers are indicated to the right of the gels. (Panels B and C) Schematic diagrams of the RNase P ribozyme secondary structure. Regions that are mapped in the accompanying gels are highlighted. Individual residues that are sensitive to one or more of the analogues surveyed are circled and the element of RNase P RNA secondary structure in which they are located are indicated in boxes adjacent to the RNA sequence.

identical patterns of nucleotide analogue sensitivity in both substrate binding (*34*, *37*) and cleavage interference assays, and all are located in the C-domain. In contrast, A136 and A232−234, which are found in the S-domain, are only sensitive to analogue interference in substrate binding. The positions that contribute to catalysis cluster near the pre-tRNA cleavage site in current models of the RNase P ribozyme−substrate complex (Figure 9; see the following discussion). Interestingly, several of the positions detected are also located adjacent to the phosphorothioate-sensitive residues in P4 identified as positions of divalent metal ion coordination (A62−A65 in J3/4 and A351 in J2/4). The low metal ion conditions required in order to detect interference in J3/4 and J2/4 and their proximity to P4 suggest that some of the interference results could reflect a disruption of functionally important divalent metal ion interactions within the C-domain.

Analysis of the Mg^{2+} and pH Dependence of PT332(-5) and PT50 Ribozyme Reactions. Because the PT332(-5) and PT50 self-cleavage reactions employed in the NAIM analysis are initiated by the addition of Mg^{2+}, multiple Mg^{2+}-dependent steps such as folding and substrate docking must occur before catalysis (*41*, *42*). Obviously, such factors will influence the results of introducing chemical modifications at residues involved in ribozyme structure and function. Given the involvement of metal ion interactions in folding, substrate binding, and catalysis and the propensity of RNAs to undergo slow structural transitions (*43*, *44*), the same step might not always be rate-limiting under different metal ion concentrations. Thus, it is possible that the differential sensitivity to analogue interference at different Mg^{2+} concentrations might reflect a change in rate-limiting step. To further explore the nature of the rate-limiting step for cleavage of PT50 and PT332(-5), we examined the pH dependence of the reaction rate at 1.25, 25, and 150 mM Mg^{2+} (Figure 7A).

We reasoned that because the single turnover reaction catalyzed by the native enzyme is pH dependent and this dependence is linear over the range of pH 5.5−7.5 (*45*), we may detect changes in rate-limiting step as a change in the pH dependence of the reaction. Previously, we showed that, like the native ribozyme, the reaction-rate constants of PT332(-5) and PT50 at 25 mM $MgCl_2$ are also linearly dependent on pH, with slope of 0.81 for PT50 and 0.88 for PT332(-5) (*22*) (Figure 7A). Figure 7A shows that, even at Mg^{2+} concentrations as low as 1.25 mM, the reaction rate retains pH sensitivity (with slopes of 0.84 for PT50 and 0.88 for PT332(-5)), indicating that a pH-independent step such as folding, substrate docking, or a conformational change has not become rate-limiting at these relatively low Mg^{2+}

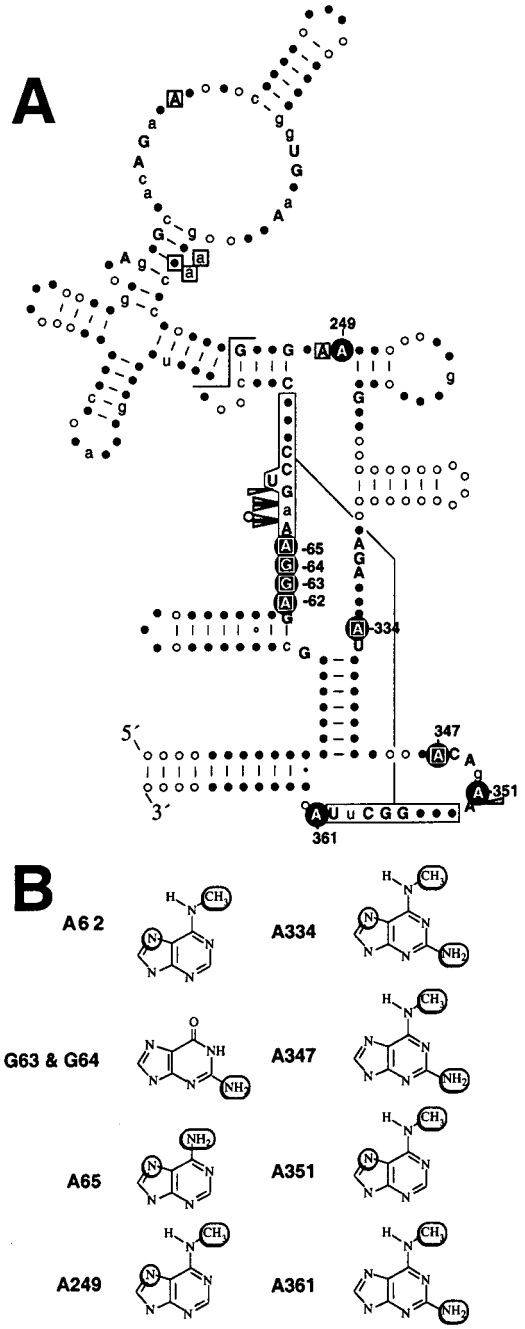

FIGURE 6: Compilation of NAIM data for the RNase P ribozyme from *E. coli*. (A) The results obtained with *E. coli* RNase P RNA are shown in the context of the bacterial consensus secondary structure (*24*). Individual nucleotide positions that are found in >90% of the bacterial RNase P RNAs are depicted as circles. Nucleotide positions where base identity is universally conserved are shown as capital letters. Nucleotide positions that are conserved in at least 90% of the known RNase P RNAs are shown as lower case letters. Arrowheads show the locations of phosphate oxygens where sulfur substitution disrupts catalytic activity. A circle adjacent to the arrowhead at A67 indicates the phosphorothioate modification at this position can be completely rescued by thiophilic divalent metal ions. Nucleotides that were found to be sensitive in the self-cleavage assay to one or more of the analogues tested are circled and the corresponding residue number in *E. coli* RNase P RNA is indicated. Residues that were sensitive to analogue interference in substrate binding (*36*) are indicated by boxes. (B) The modifications at individual nucleotides that give rise to interference effects are shown. The residue number in *E. coli* RNase P RNA is shown at left. For each of the individual residues where interference was detected, the individual functional group where modification gives rise to a significant interference effect is highlighted.

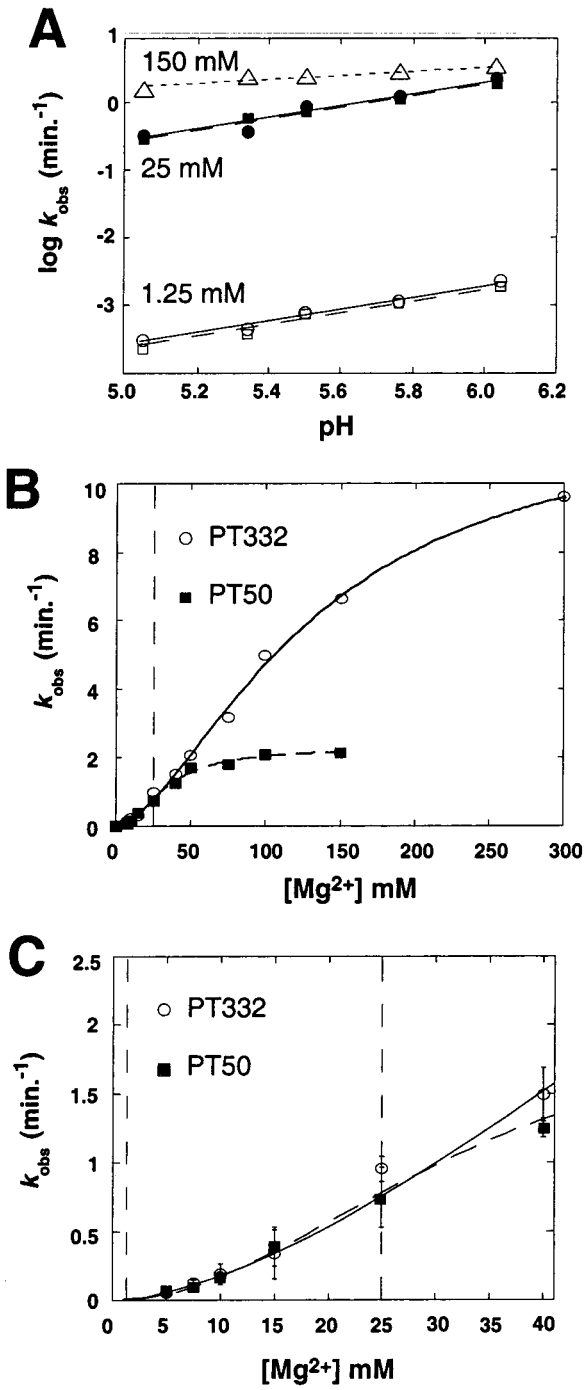

FIGURE 7: pH and Mg^{2+} dependence of PT50 and PT332(-5) self-cleavage. (A) pH dependence of the PT50 and PT332(-5) ribozyme reactions. Data for the PT50 ribozyme at 1.25 mM (open squares), 25 mM (filled squares), and 150 mM Mg^{2+} (triangles) are shown by dashed lines. Data for PT332(-5) at 1.25 mM (open circles) and 25 mM Mg^{2+} (filled circles) are shown by solid lines. Data were fit to a linear equation to derive the slopes described in the text. (B) Dependence of k_{obs} on Mg^{2+} ion concentration for PT50 (filled squares) and PT332(-5) (open circles). The data are fit to the Hill equation, yielding an n value of 1.63 (0.09) and Mg_{50} of 131 (1.9) mM for PT332(-5) and an n value of 2.07 (0.17) and Mg_{50} of 33.6 (1.9) mM for PT50. Values in parentheses are the standard error from the curve fit for the respective parameters. (C) A detail of the data presented in B showing the Mg^{2+} dependence of PT50 and PT332(-5) reactions at low Mg^{2+} concentration. Dashed vertical lines indicate concentrations of 1.25 and 25 mM Mg^{2+} that were employed in subsequent NAIM experiments. Error bars represent ±1 standard deviation of the average of at least three experiments.

concentrations. Thus, the increased sensitivity of the ribozyme to analogue interference does not appear to be due to a change in ribozyme kinetics but may reflect a more direct coupling between the sensitive functional groups and divalent metal ion interactions.

To better understand the relationship between the metal ion concentrations required to engender interference effects and the overall affinity of the ribozyme for Mg^{2+}, we determined the dependence of the PT332(-5) and PT50 reaction rates on divalent metal ion concentration. Plots of k_{obs} for PT50 and PT332(-5) cleavage reactions as a function of Mg^{2+} concentration show that the reactions of both ribozymes are cooperatively dependent on divalent metal ion (Figure 7B). Plots of k_{obs} versus Mg^{2+} ion concentration for both constructs fit well to a cooperative binding isotherm (eq 3), giving a Hill number of approximately 2, similar to the untethered native reaction (*41*, *46*). However, k_{obs} for PT50 and PT332(-5) reactions differ in their rates at saturating concentrations of Mg^{2+}. At low pH (5.5), the maximal rate of reaction is 2 min^{-1} for PT50 and 15 min^{-1} for PT332(-5); however, the rates are essentially identical up to ca. 40 mM Mg^{2+} (Figure 7C). A potential explanation for this difference is provided by the observation that at 150 mM Mg^{2+} the PT50 reaction shows a marked decrease in its dependence on pH ($m = 0.88$ at 25 mM Mg^{2+}; $m = 0.35$ at 150 mM Mg^{2+}). The reaction rate for PT332(-5) is too fast to measure manually at higher pH values under conditions of 150 mM Mg^{2+}. However, these data are consistent with the interpretation that, at Mg^{2+} concentrations up to ca. 40 mM, PT50 and PT332(-5) share the same pH dependent rate-limiting step but that, at higher metal ion concentrations, there is a change to a less pH dependent rate-limiting step for the PT50 ribozyme.

Effects of Site-Specific Functional Group Modification on RNase P Ribozyme Catalysis. The relatively high concentrations of Mg^{2+} required for saturation suggest that an important class of low-affinity metal ion interactions contributes to RNase P ribozyme catalysis under these conditions. On the other hand, the relatively low concentrations of metal ion required to engender sensitivity to analogue interference appears most consistent with linkage of these effects to higher-affinity metal ion interactions. Although NAIM is a very powerful method for rapidly identifying important functional groups, it is difficult to obtain quantitative information about the contribution of the groups detected. Therefore, to explore in detail the relationship between Mg^{2+} binding and the effects of functional group modification, we constructed a series of site-specifically modified ribozymes on the basis of NAIM results. We focused on functional groups in the J3/4 region of the ribozyme because this element is universally conserved in sequence and sequence-length in bacterial RNase P RNAs and is adjacent to the nucleotides in P4 that are involved in divalent metal ion interactions important for catalysis (*21*, *22*). In the present study, we examined modification of the N7 position of purines in J3/4 because this functional group is often an outer sphere ligand for hydrated metal ion interactions with RNA (*47*). Additionally, we examined modifications at the phosphorothioate sensitive positions in P4 because these functional groups cannot be examined using NAIM because of the masking effect of the sulfur substitution.

Table 1 shows the rate constants for ribozymes with N7-deaza-2′-deoxyadenosine (7ddA) or N7-deaza-2′-deoxyguanosine modifications at positions A62, G63, A65, A66, A67, and G68. Because modification of the N7 position necessitated making a corresponding 2′-deoxy modification at the same nucleotide (see Materials and Methods), we also analyzed the effects of modification at the 2′ position alone in those cases where effects were observed with the double modification. We find that, at 2.5 mM Mg^{2+} only, modifications at positions A62, A65, and A66 resulted in catalytic defects attributable to changing the N7 nitrogen to a carbon, which is similar to the pattern of sensitivity in NAIM. Additionally, we determined the effect of N7-deaza modification at A66, G68, and A67 that could not be examined by NAIM because of interfering phosphorothioate effects at these positions; however, modifications at G68 and A67 did not appreciably affect the rate of reaction. In contrast, A66 was found to be sensitive to changing the N7 nitrogen to carbon.

For A62 and A65, the interference effect was solely attributed to modification at the N7 position because the corresponding 2′-deoxy modifications at these positions had no measurable effect on reaction rate. However, a 2′-deoxy modification at A66 results in a 5−6-fold increase in ribozyme catalytic rate. A lesser degree of enhancement in reaction rate is observed with the combined N7-deaza-2′-deoxyadenosine modification. Assuming that the effects of modification at the N7 and 2′ positions are independent, the defect due to N7 modification can be obtained by normalizing to the rate of the ribozyme with the 2′-deoxy modification alone. This yields a small (ca. 2-fold) but measurable interference effect due to N7 modification at A66 (Table 1). These results confirm the NAIM data and support the interpretation that the additional interferences observed at other sites in the C-domain represent similar 2−4-fold defects in the catalytic rate.

Importantly, the ability to monitor reaction kinetics also permits a more detailed examination of the effects of changes in Mg^{2+} concentration. We determined the effect of increasing Mg^{2+} concentration from 2.5 to 25 mM on the rate constants for the modified ribozymes (Table 1 and Figure 8). As expected, the rate constant of the unmodified ribozyme is larger at the higher Mg^{2+} concentration (0.01 min^{-1} at 2.5 mM versus 0.55 min^{-1} at 25 mM Mg^{2+} (pH 5.5)). We controlled for this intrinsic difference in reaction rate due to increased metal ion concentration by normalizing the effect of ribozyme modification to the rate of the unmodified ribozyme (Table 1). We find that the effects of N7-deazaadenosine modification at A62 and A66 decrease moderately at 25 mM Mg^{2+}, as might be expected because of the general effect of structural stabilization by increasing metal ion concentration. In contrast, the effect of carbon substitution of the N7 of A65 is entirely suppressed under these conditions.

Figure 8 shows a direct comparison of the reaction kinetics of the native PT50 ribozyme and PT50 ribozymes with individual 7ddA modifications at A65 and A62. At 2.5 mM Mg^{2+}, modification of the N7 position of either A62 or A65 results in a measurable decrease in the rate of ribozyme catalysis. However, when the reactions are examined at 25 mM Mg^{2+}, the rate of the 7ddA65 ribozyme is essentially indistinguishable from the native PT50 ribozyme. Modifica-

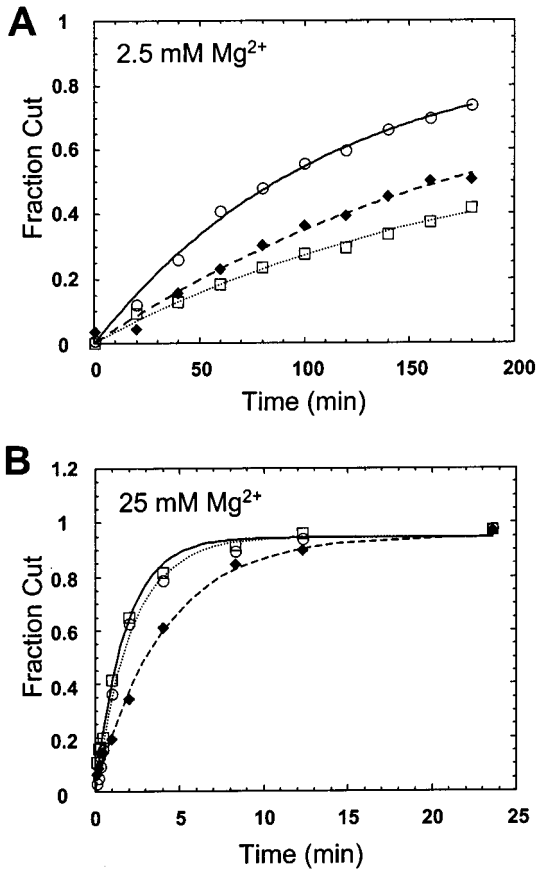

FIGURE 8: Effects of N7-deazaadenosine modification in J3/4 on RNase P ribozyme reaction kinetics. Plot of fraction RNA reacted versus time is shown for unmodified PT50 (circles) and for ribozymes with N7ddA modifications at A62 (diamonds) and A65 (squares). The data are fit to a single-exponential function, as described in Materials and Methods. Panels A and B display data obtained at 2.5 and 25 mM Mg^{2+}, respectively.

tion at A62 still results in a detectable decrease in the rate of ribozyme self-cleavage under these conditions; however, the effect is decreased to only 2-fold. These distinct sensitivities to metal ion concentration under the high monovalent ion conditions employed argue against general structural stabilization by Mg^{2+} but are more consistent with a specific linkage between structure involving the N7 position of A65 and metal ion binding.

DISCUSSION

An important aspect of the reaction conditions employed in these studies is that high-affinity interaction between native RNase P RNA and its substrate in the absence of protein requires relatively high concentrations of monovalent ions (*41*, *48*). Both self-cleaving ribozymes share this requirement for high ionic strength in that, at lower monovalent ion concentrations, the fraction of reactive RNA decreases significantly (Kaye and Harris, unpublished work). Under these conditions, the electrostatic repulsive forces that act to disrupt RNA structure are likely to be largely suppressed and any nonspecific electrostatic interaction of Mg^{2+} ions is likely to be significantly weakened (*49*). Monovalent ions can also compete, to a lesser extent, with site-specific metal ion binding; however, they cannot entirely replace specific structural and catalytic roles afforded by divalent metal ion contacts with nucleotide and base functional groups.

Under "optimal" reaction conditions of 15−25 mM Mg^{2+}, none of the base functional groups examined appears to make a large thermodynamic contribution to ribozyme catalysis (>2-fold) on the basis of the interference results. It is likely that this behavior reflects monovalent ion screening of repulsive electrostatic forces, which would minimize the disruptive effect of modification. The small number of base functional groups detected is also likely a result of the significant structural stabilization afforded by structurally complex large ribozymes, in particular at high monovalent ion conditions (*50*, *51*). This may explain why the interference assay involving ribozyme self-cleavage does not detect known elements of tertiary structure such as the loop−helix interactions between L18 and P8, as well as L9 and P1 (*52*, *53*), which are detected in interference studies that rely on gel-mobility shift to isolate ribozymes competent to bind substrate (*34*). Small perturbations of structure in these phylogenetically variable peripheral elements apparently do not cause sufficient structural destabilization to engender a significant decrease in the reaction rate under the high-monovalent but low-divalent metal ion conditions.

In contrast, under such conditions, the ribozyme is appreciably sensitive to modification at a subset of highly conserved residues in the C-domain. The requirement for such low metal ion concentrations relative to the overall apparent affinity for Mg^{2+} suggests that the functional groups identified participate either directly or indirectly in structure involving high-affinity metal ion interactions. Notably, the level of Mg^{2+} required to engender interference effects at these sites is within the general range of metal ion concentrations (2−3 mM) required for folding of RNase P RNA (*4*, *42*, *44*). Additionally, similar concentrations of divalent metal ions are required for folding of Group I and Group II ribozymes (*50*). The apparent affinities of individual metal ion interactions at the reactive phosphate of the Group I ribozyme are also in the range of ca. 0.1−5 mM (*54*, *55*); however, like the RNase P ribozyme, maximal catalytic rates require somewhat higher Mg^{2+} ion concentrations (*41*, *56*). Thus, mapping residues under conditions of low Mg^{2+}, to engender weakening of Mg-dependent structure, while suppressing general effects of structural perturbation with high concentrations of monovalent ions may effectively restrict the functional groups detected to those with roles more directly related or coupled to site-specific Mg^{2+} interactions.

On the basis of the general arrangement of nucleotides in the low-resolution models and the interference results reported here, a general topology of the C-domain relative to the pre-tRNA cleavage site and a description of the contributions of individual elements to ribozyme catalysis can be proposed. As shown in Figure 6, the functional groups important for catalysis identified here cluster adjacent to the pre-tRNA cleavage site at the base of the acceptor stem. The functional groups that contribute to catalysis are located in two general regions in the C-domain: in J5/15, which is adjacent to the site of CCA binding in P15, and at the interface between helical elements P1−P4 and P2−P3 in the multihelix junction formed by P1−P4.

The close association of the J5/15 element with the pre-tRNA cleavage site was demonstrated by short-range cross-linking (*12*, *14*, *57*), as well as its obvious proximity to the site of CCA binding in P15 (*15*, *16*, *58*) (Figure 9A). Previous interference studies showed that the adenosine base

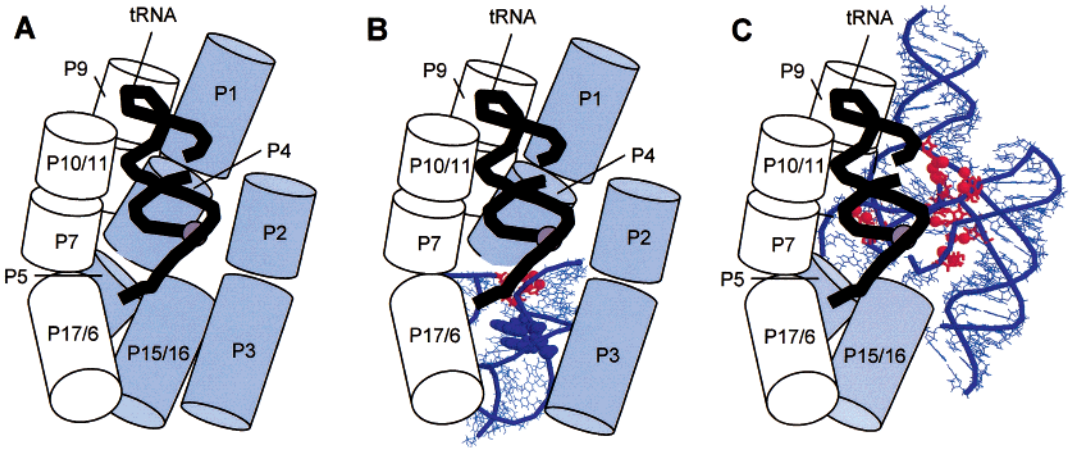

FIGURE 9: Location of analogue sensitive functional groups in models of the RNase P ribozyme−substrate complex. (A) Schematic representations of the *E. coli* RNase P ribozyme−substrate complex on the basis of available structure models (*11*, *53*). The helices that make up the C-domain are shown in blue, while the helices that are included in the S-domain are shown in white. The position of the bound tRNA is shown by a black ribbon and the location of the 5′ end of tRNA is depicted by a gray sphere. (B) Location of important functional groups in J5/15. The individual nucleotides in J5/15, P15, and P16 are shown in wireframe, and sensitive functional groups are shown in red. The nucleotides in P15 that contact the 3′-CCA sequence of tRNA are shown in blue and depicted in space filling representation. (C) Location of important functional groups in the P1−P4 multihelix junction. The individual nucleotides encompassed in the P1−P4 element are shown in wireframe as in panel B. The path of the phosphodiester backbone is indicated by a blue ribbon. Nucleotides that participate in catalytic function are shown in red, and the individual functional groups detected in the NAIM analysis are shown in space filling representation.

at A248 in J5/15 is important for substrate binding (*37*), and the joint contribution of this region to enzyme function is also observed with mutations in J5/15 which can have large effects on both binding and catalysis (Zahler and Harris, unpublished work). Additionally, miscleavage can be engendered by mutations in J5/15 (Zahler and Harris, unpublished work), as has been shown previously for mutations in P15 that disrupt interactions with the tRNA 3′-CCA sequence (*15*). Also, in models of the structure of the ribozyme−substrate complex, the J5/15 and P15 regions are located on the minor groove side of the acceptor stem (*11*, *53*, *59*) (Figure 9). Taken together, the cross-linking, interference, kinetic, and thermodynamic data indicate that J5/15 functions to make direct contacts with the substrate and facilitates selection of the appropriate phosphodiester bond. Although the precise interactions between J5/15 and the cleavage site have yet to be established, the pattern of analogue interference at A248 and A249 indicate that such interactions involve the major groove edge of these residues.

The majority of the functional groups identified by NAIM using cleavage for selection are located at universally conserved residues in the joining regions within the multihelix junction composed of P1−P4 (Figure 9B). Like J5/15, the P1−P4 element is positioned proximal to the base of the pre-tRNA acceptor stem but opposite the major rather than minor groove (*11*, *53*, *60*, *61*). The fact that most of the conserved nucleotide positions in the C-domain are located in P1−P4 also supports an important role for this element in ribozyme function (*24*, *25*, *62*). Substrate binding is also sensitive to analogue substitution in the P1−P4 element, and the interferences overlap significantly with the pattern observed in this analysis (*37*) (Figures 1 and 7). Additionally, there is recent evidence for direct interactions between residues in P1−P4 and divalent metal ions that are important for catalysis (*22*) (Christian et al., submitted for publication). Thus, several lines of evidence support a role for P1−P4 functional groups in tertiary interactions, substrate binding, and catalysis.

Given the relative orientations of P3 and P4 in both models, the J3/4 element forms a sharp turn bringing the important functional groups at G64, G63, and A62 in close proximity to the sites of metal ion interaction in P4 (see the following discussion). Interestingly, the enhancement of cleavage rate we observe because of 2′-deoxyadenosine modification at A66 may be due to the conformation of the phosphodiester backbone in the region. Similar enhancements due to C2′ modification in other ribozymes have been observed at positions where ribose ring pucker is important for the active topology (*63*). Within the RNase P RNA secondary structure, nucleotide A65 is adjacent to, and may pair with, A361, and both nucleotides show interference effects. For A65, the interference data indicate the involvement of N7 and N6, while the sensitivity of A361 to DAPαS, PuraS, and ^{NME}AαS suggest it is the Watson−Crick edge of this nucleotide that is important for function. On the basis of the relative orientation of these nucleotides, an A−A pair involving the Hoogsteen edge of A65 and the Watson−Crick binding edge of A361 could be accommodated given the global arrangement of the currently available structure models (Harris, unpublished work). Importantly, all of the functional groups in P4 and J3/4 detected as contributing to catalysis also appear to function in substrate binding (*37*).

The interference results also detected purine functional groups important for catalysis in the J18/2 and J2/4 regions of the C-domain (Figure 9). Similar sensitivity to analogue modification due to disruption of substrate binding was also mapped to these regions, however, there is only partial overlap with the NAIM results employing self-cleavage selection. Identical results are obtained using both approaches for nucleotide A334 in J18/2, demonstrating sensitivity to modification of N6 and N7 and introduction of an N2 amine (*35*, *37*). A role for J18/2 in substrate cleavage is also suggested by mutational studies involving this region showing effects on both ground-state binding and catalysis (*64*, *65*). Consistent with these observations, A334 cross-links to the proximal portion of the 5′ leader sequence (*13*, *14*) and

has been demonstrated to be in proximity to the RNase P protein (*18*). Additionally, the 5′ leader sequence protects nucleotides in J18/2 from chemical modification (*16*), suggesting that this region may participate in 5′ leader sequence recognition in conjunction with the RNase P protein, which contacts this portion of pre-tRNA (*19*, *66*).

In contrast, differences in the contribution of functional groups to binding and catalysis are observed in J2/4. Only A347 was detected as contributing to substrate binding in NAIM analysis employing selection using biotinylated pre-tRNA substrates (*37*), while both A347 and A351 show sensitivity in the self-cleavage results described here. A distinct pattern of sensitivity is observed in binding interference experiments that employ gel-mobility shift separation of bound and unbound RNAs, which appear to be more sensitive to perturbation of tertiary structure (*34*, *35*). The larger collection of N7-deazaadenosine and phosphorothioate interference effects identified in these studies encompasses essentially all of the more restricted subset of NAIM results reported previously. However, differences in J2/4 are apparent in that A351 and A349, instead of A351 and A347, are sensitive to modification of the N7 nitrogen. The condition dependence of interference effects in J2/4 unfortunately makes it difficult to rationalize the data in terms of specific aspects of structure, even though the available structure models position this element adjacent to the bound substrate. Additionally, a role for J2/4 in metal ion interactions is consistent not only with the NAIM results but also with the proximity of these nucleotide base functional groups to the very strong phosphorothioate effect observed at A352 (*21*, *22*).

The sensitivity of the interference signal to Mg^{2+} concentrations and the proximity of the functional groups detected to sites of metal ion interaction in P4 suggests that one contribution of these conserved sequences is in formation of Mg^{2+}-dependent structure of the P1−P4 multihelix junction. Insight into the structures associated with metal ion binding in RNA is provided by high-resolution structures of several RNAs, including tRNA (*67*, *68*), 5S rRNA (*69*), and the P4−P6 domain of the Group I intron (*70*). These structures reveal that Mg^{2+} ions tend to cluster in regions of complex RNA tertiary structure where packing constraints bring the negatively charged phosphate backbone into proximity; a similarly complex and compact structure incorporating site-specific metal ion interactions is expected in the P1−P4 element.

Recent evidence for participation of P1−P4 chemical groups in metal ion interactions is provided by quantitative analysis of thiophilic metal ion rescue of phosphorothioate interference at A67 in P4 (*22*) (Christian et al., submitted for publication). Thiophilic metal rescue of sulfur effects at nonbridging oxygens provides evidence for direct metal ion coordination (*38*, *71*). Site-specific modification of the N7 position of A66 significantly weakens the apparent affinity for metal ions bound at A67, while modification of A65 reveals the presence of an additional metal ion bound in J3/4 with an apparent dissociation constant in the micromolar range. This interpretation is consistent with the differential sensitivity of ribozymes modified at A65 and A66 to Mg^{2+} concentration in that effects at A65 are suppressed at relatively low metal ion concentrations while the effect of modification at A66 appears to require higher concentrations of Mg^{2+}. Also, binding of the transition metal terbium, which can, in some instances, overlap with Mg^{2+} binding sites (*72*−*74*), results in specific cleavage in J3/4, providing additional evidence that functional groups in this region are involved in metal ion coordination (Kaye et al., submitted for publication). Taken together, the available information suggests that the contribution of the P1−P4 multihelix junction is to position metal ions that are important for catalysis, an important aspect of which may be to position Mg^{2+} ions that interact with the substrate cleavage site.

ACKNOWLEDGMENT

We gratefully acknowledge the advice and encouragement of Adam Cassano and Nathan Zahler during these studies, as well as for careful reading of the manuscript. We thank Dr. Stephen L. Hajduk for assistance in the synthesis of RNA oligonucleotides. Additionally, we thank Dr. Scott Strobel and his laboratory for generously providing nucleotide analogue phosphorothioates, as well as for sharing expertise on application of NAIM.

REFERENCES

1. Kurz, J. C., and Fierke, C. A. (2000) *Curr. Opin. Chem. Biol. 4*, 553−558.
2. Frank, D. N., and Pace, N. R. (1998) *Annu. Rev. Biochem. 67*, 153−180.
3. Guerrier-Takada, C., Gardiner, K., Marsh, T., Pace, N., and Altman, S. (1983) *Cell 35*, 849−857.
4. Pan, T. (1995) *Biochemistry 34*, 902−909.
5. Loria, A., and Pan, T. (1996) *RNA 2*, 551−563.
6. Loria, A., and Pan, T. (1997) *Biochemistry 36*, 6317−6325.
7. Odell, L., Huang, V., Jakacka, M., and Pan, T. (1998) *Nucleic Acids Res. 26*, 3717−3723.
8. Mobley, E. M., and Pan, T. (1999) *Nucleic Acids Res. 27*, 4298−4304.
9. Qin, H., Sosnick, T. R., and Pan, T. (2001) *Biochemistry 40*, 11202−11210.
10. Nolan, J. M., Burke, D. H., and Pace, N. R. (1993) *Science 261*, 762−765.
11. Chen, J. L., Nolan, J. M., Harris, M. E., and Pace, N. R. (1998) *EMBO J. 17*, 1515−1525.
12. Christian, E. L., McPheeters, D. S., and Harris, M. E. (1998) *Biochemistry 37*, 17618−17628.
13. Christian, E. L., and Harris, M. E. (1999) *Biochemistry 38*, 12629−12638.
14. Burgin, A. B., and Pace, N. R. (1990) *EMBO J. 9*, 4111−4118.
15. Kirsebom, L. A., and Svard, S. G. (1994) *EMBO J. 13*, 4870−4876.
16. LaGrandeur, T. E., Huttenhofer, A., Noller, H. F., and Pace, N. R. (1994) *EMBO J. 13*, 3945−3952.
17. Oh, B. K., Frank, D. N., and Pace, N. R. (1998) *Biochemistry 37*, 7277−7283.
18. Biswas, R., Ledman, D. W., Fox, R. O., Altman, S., and Gopalan, V. (2000) *J. Mol. Biol. 296*, 19−31.
19. Niranjanakumari, S., Stams, T., Crary, S. M., Christianson, D. W., and Fierke, C. A. (1998) *Proc. Natl. Acad. Sci. U.S.A. 95*, 15212−15217.
20. Crary, S. M., Niranjanakumari, S., and Fierke, C. A. (1998) *Biochemistry 37*, 9409−9416.
21. Harris, M. E., and Pace, N. R. (1995) *RNA 1*, 210−218.
22. Christian, E. L., Kaye, N. M., and Harris, M. E. (2000) *RNA 6*, 511−519.
23. Frank, D. N., and Pace, N. R. (1997) *Proc. Natl. Acad. Sci. U.S.A. 94*, 14355−14360.
24. Brown, J. W. (1999) *Nucleic Acids Res. 27*, 314.
25. Chen, J. L., and Pace, N. R. (1997) *RNA 3*, 557−560.
26. Ryder, S. P., Ortoleva-Donnelly, L., Kosek, A. B., and Strobel, S. A. (2000) *Methods Enzymol. 317*, 92−109.

27. Szewczak, A. A., Ortoleva-Donnelly, L., Zivarts, M. V., Oyelere, A. K., Kazantsev, A. V., and Strobel, S. A. (1999) *Proc. Natl. Acad. Sci. U.S.A. 96*, 11183−11188.
28. Basu, S., Rambo, R. P., Strauss-Soukup, J., Cate, J. H., Ferre-D'Amare, A. R., Strobel, S. A., and Doudna, J. A. (1998) *Nat. Struct. Biol. 5*, 986−992.
29. Ryder, S. P., Oyelere, A. K., Padilla, J. L., Klostermeier, D., Millar, D. P., and Strobel, S. A. (2001) *RNA 7*, 1454−1463.
30. Kazantsev, A. V., and Pace, N. R. (1998) *RNA 4*, 937−947.
31. Hardt, W. D., Warnecke, J. M., Erdmann, V. A., and Hartmann, R. K. (1995) *EMBO J. 14*, 2935−2944.
32. Hardt, W. D., Warnecke, J. M., and Hartmann, R. K. (1995) *Mol. Biol. Rep. 22*, 161−169.
33. Hardt, W. D., Erdmann, V. A., and Hartmann, R. K. (1996) *RNA 2*, 1189−1198.
34. Heide, C., Pfeiffer, T., Nolan, J. M., and Hartmann, R. K. (1999) *RNA 5*, 102−116.
35. Heide, C., Feltens, R., and Hartmann, R. K. (2001) *RNA 7*, 958−968.
36. Frank, D. N., Harris, M. E., and Pace, N. R. (1994) *Biochemistry 33*, 10800−10808.
37. Siew, D., Zahler, N. H., Cassano, A. G., Strobel, S. A., and Harris, M. E. (1999) *Biochemistry 38*, 1873−1883.
38. Eckstein, F., and Gish, G. (1989) *Trends Biochem. Sci. 14*, 97−100.
39. Gish, G., and Eckstein, F. (1988) *Science 240*, 1520−1522.
40. Pfeiffer, T., Tekos, A., Warnecke, J. M., Drainas, D., Engelke, D. R., Seraphin, B., and Hartmann, R. K. (2000) *J. Mol. Biol. 298*, 559−565.
41. Beebe, J. A., Kurz, J. C., and Fierke, C. A. (1996) *Biochemistry 35*, 10493−10505.
42. Pan, T., and Sosnick, T. R. (1997) *Nat. Struct. Biol. 4*, 931−938.
43. Russell, R., and Herschlag, D. (1999) *J. Mol. Biol. 291*, 1155−1167.
44. Zarrinkar, P. P., Wang, J., and Williamson, J. R. (1996) *RNA 2*, 564−573.
45. Smith, D., and Pace, N. R. (1993) *Biochemistry 32*, 5273−5281.
46. Smith, D., Burgin, A. B., Haas, E. S., and Pace, N. R. (1992) *J. Biol. Chem. 267*, 2429−2436.
47. Feig, A. L., and Uhlenbeck, O. C. (1999) in *The RNA World 2*, pp 287−320, CSH Press, Cold Spring Harbor, NY.
48. Gardiner, K. J., Marsh, T. L., and Pace, N. R. (1985) *J. Biol. Chem. 260*, 5415−5419.
49. Misra, V. K., and Draper, D. E. (1998) *Biopolymers 48*, 113−135.
50. Celander, D. W., and Cech, T. R. (1991) *Science 251*, 401−407.
51. Heilman-Miller, S. L., Thirumalai, D., and Woodson, S. A. (2001) *J. Mol. Biol. 306*, 1157−1166.
52. Brown, J. W., Nolan, J. M., Haas, E. S., Rubio, M. A., Major, F., and Pace, N. R. (1996) *Proc. Natl. Acad. Sci. U.S.A. 93*, 3001−3006.
53. Massire, C., Jaeger, L., and Westhof, E. (1998) *J. Mol. Biol. 279*, 773−793.
54. Shan, S., Kravchuk, A. V., Piccirilli, J. A., and Herschlag, D. (2001) *Biochemistry 40*, 5161−5171.
55. Shan, S., Yoshida, A., Sun, S., Piccirilli, J. A., and Herschlag, D. (1999) *Proc. Natl. Acad. Sci. U.S.A. 96*, 12299−12304.
56. McConnell, T. S., Herschlag, D., and Cech, T. R. (1997) *Biochemistry 36*, 8293−8303.
57. Kufel, J., and Kirsebom, L. A. (1996) *Proc. Natl. Acad. Sci. U.S.A. 93*, 6085−6090.
58. Oh, B. K., and Pace, N. R. (1994) *Nucleic Acids Res. 22*, 4087−4094.
59. Harris, M. E., Nolan, J. M., Malhotra, A., Brown, J. W., Harvey, S. C., and Pace, N. R. (1994) *EMBO J. 13*, 3953−3963.
60. Harris, M. E., Kazantsev, A. V., Chen, J. L., and Pace, N. R. (1997) *RNA 3*, 561−576.
61. Harris, M. E., and Christian, E. L. (1999) *Methods 18*, 51−59.
62. Harris, J. K., Haas, E. S., Williams, D., Frank, D. N., and Brown, J. W. (2001) *RNA 7*, 220−232.
63. Ryder, S. P., and Strobel, S. A. (1999) *J. Mol. Biol. 291*, 295−311.
64. Hardt, W. D., and Hartmann, R. K. (1996) *J. Mol. Biol. 259*, 422−433.
65. Schlegl, J., Hardt, W. D., Erdmann, V. A., and Hartmann, R. K. (1994) *EMBO J 13*, 4863−4869.
66. Kurz, J. C., Niranjanakumari, S., and Fierke, C. A. (1998) *Biochemistry 37*, 2393−2400.
67. Jack, A., Ladner, J. E., and Klug, A. (1976) *J. Mol. Biol. 108*, 619−649.
68. Jack, A., Ladner, J. E., Rhodes, D., Brown, R. S., and Klug, A. (1977) *J. Mol. Biol. 111*, 315−328.
69. Correll, C. C., Freeborn, B., Moore, P. B., and Steitz, T. A. (1997) *Cell 91*, 705−712.
70. Cate, J. H., and Doudna, J. A. (1996) *Structure 4*, 1221−1229.
71. Pecoraro, V. L., Hermes, J. D., and Cleland, W. W. (1984) *Biochemistry 23*, 5262−5271.
72. Lee, N., and Suga, H. (2001) *Biochemistry 40*, 13633−13643.
73. Sigel, R. K., Vaidya, A., and Pyle, A. M. (2000) *Nat. Struct. Biol. 7*, 1111−1116.
74. Feig, A. L., Scott, W. G., and Uhlenbeck, O. C. (1998) *Science 279*, 81−84.
75. Strobel, S. A. (1999) *Curr. Opin. Struct. Biol. 9*, 346−52.

BI012158H